photonics

MDPI

Article

Mid-Infrared Continuous Varifocal Metalens with Adjustable Intensity Based on Phase Change Materials

Liangde Shao [1,2,3], Kongsi Zhou [1,2,3], Fangfang Zhao [1], Yixiao Gao [1,2,3,*], Bingxia Wang [1,2,3] and Xiang Shen [1,2,3,*]

[1] The Research Institute of Advanced Technologies, Ningbo University, Ningbo 315211, China
[2] Key Laboratory of Photoelectric Detection Materials and Devices of Zhejiang Province, Ningbo 315211, China
[3] Engineering Research Center for Advanced Infrared Photoelectric Materials and Devices of Zhejiang Province, Ningbo University, Ningbo 315211, China
* Correspondence: gaoyixiao@nbu.edu.cn (Y.G.); shenxiang@nbu.edu.cn (X.S.)

Abstract: Metalenses can greatly reduce the complexity of imaging systems due to their small size and light weight and also provide a platform for the realization of multifunctional imaging devices. Achieving dynamic focus length tunability is highly important for metalens research. In this paper, based on single-crystal Ge and a new low-loss phase change material $Ge_2Sb_2Se_5$ (GSSe), a tunable metalens formed by a double-layer metasurface composite was realized in the mid-infrared band. The first-layer metasurface formed by Ge nanopillars combines propagation and the geometric phase (equivalent to a half-wave plate function) to produce single- or multiple-polarization-dependent foci. The second-layer metasurface formed by GSSe nanopillars provides a tunable propagation phase, and the double-layer metalens can achieve the tunability of the focus length depending on the different crystalline fractions of GSSe. The focal length varies from 62.91 to 67.13 μm under right circularly polarized light incidence and from 33.84 to 36.66 μm under left circularly polarized light incidence. Despite the difference in the crystallographic fraction, the metalens's focusing efficiency is maintained basically around 59% and 48% when zooming under RCP and LCP wave excitation. Meanwhile, the incident wave's ellipticity can be changed to alter the relative intensity ratios of the bifocals from 0.03 to 4.26. This continuous varifocal metalens with adjustable intensity may have potential in practical applications such as optical tomography, multiple imaging, and systems of optical communication.

Keywords: mid-infrared band; reconfigurable metalens; phase change material $Ge_2Sb_2Se_5$; continuous zoom; adjustable intensity ratios

check for updates

Citation: Shao, L.; Zhou, K.; Zhao, F.; Gao, Y.; Wang, B.; Shen, X. Mid-Infrared Continuous Varifocal Metalens with Adjustable Intensity Based on Phase Change Materials. *Photonics* **2022**, *9*, 959. https://doi.org/10.3390/photonics9120959

Received: 7 November 2022
Accepted: 8 December 2022
Published: 9 December 2022

Publisher's Note: MDPI stays neutral with regard to jurisdictional claims in published maps and institutional affiliations.

Copyright: © 2022 by the authors. Licensee MDPI, Basel, Switzerland. This article is an open access article distributed under the terms and conditions of the Creative Commons Attribution (CC BY) license (https://creativecommons.org/licenses/by/4.0/).

1. Introduction

A metasurface, a man-made, two-dimensional material consisting of an array of subwavelength optical antennas of differently shaped structures, acts like a scalpel and can "prune" electromagnetic waves such as changing their phase, amplitude, and polarization [1–4]. In recent years, various ultra-thin optical devices such as focusing lenses [5–11], holographic plates [12,13], polarization converters [14–16], and vortex phase plates [17–20] have been realized based on metasurface wavefront shaping technology. A metalens, as a subclass of metasurfaces, is a planar optical device that converges and images by modulating the phase of incident electromagnetic waves. Compared with traditional lenses, it has a subwavelength thickness, is lightweight, has a simple structure, is low cost, has high production capacity, and can be widely used in consumer electronics, security monitoring, drones, in-vehicle systems, VR/AR, and other fields.

In previous studies, single-focus or double-focus lenses can focus the incident electromagnetic wave laterally or vertically at a fixed position, and the double-focus characteristic of double-focus lenses has important application value in the field of dual-pixel imaging [21,22] and dual-channel communication [23,24]. However, in recent years, people have tended to manufacture metalenses with a variable focus to meet various applications and needs rather than being limited to a fixed focus. As a result, various forms have emerged in the study of variable focus metalenses: mechanically stretching the substrate [25–27], adjusting the mutual angle between two chiral metasurfaces [28,29], driving the geometrical position between two separate metalenses [30,31], and exploiting a micro-electro-mechanical-system (MEMS)-integrated metasurface [32–34]. The disadvantage is that these zoom metalenses need to be mechanically stretched or moved to achieve the zooming function, and problems such as easy damage, serious mechanical wear, low yield, and a complex overall device structure may occur. While these problems could be alleviated by incorporating tunable or active materials into metalenses, including liquid crystals [35–37], graphene [38–40], and phase change materials [41–45]. the metalenses integrated with graphene or liquid crystal materials suffer from low refractive index change, as well as possible absorption loss, which make it difficult to achieve high transmittance and complete continuous zoom capability. At present, a metalens with continuous zooming has been realized in the near-infrared band based on Sb_2S_3, which achieves high focusing efficiency due to the low absorption of light by the phase change material itself [44]. In the mid-infrared band, based on the phase change materials $Ge_2Sb_2Te_5$ (GST) and $Ge_2Sb_2Se_4Te_1$ (GSST), the focal position is different in the two states without continuous change. GSSe is a new broadband transparent phase change material, which not only has ultra-low loss and high cyclability in the mid-IR compared to GST and GSST, but also has a suitable refractive index contrast between the two states to achieve continuous focus movement [46,47].

In this paper, a reconfigurable metalens with continuous zooming and adjustable focus intensity is realized for the first time in the mid-infrared band (λ = 10 μm) with the help of phase change material GSSe. We simultaneously harness the propagation phase and geometric phase (Pancharatnam–Berry (PB)), where rectangular Ge nanopillars provide propagation and PB phase control and the second layer of GSSe meta-atoms provides a propagation phase control with phase distribution tunability through the crystalline fraction of GSSe. This bilayer dielectric metasurface-bound metalens proposed in this paper can generate two focal points under LP incidence, and the focus can vary from 33.84 and 62.91 μm to 36.66 and 67.13 μm when GSSe switches between amorphous and crystalline states. In addition, for multifocal lenses, the tunability of the focus relative intensity ratio is another important factor to consider. So far, there have been several ways to achieve this. The relative intensity ratio of the two focal points can be adjusted by varying the size of the unit dimensions [48], changing the crystalline fraction of the phase change material [49], and controlling the diversity of the incident beam helicity [50]. The bilayer metalens designed in this paper can utilize different crystalline fractions of phase change materials to achieve continuous zooming of the focus and can also control the intensity contrast of the bifocals by changing the phase difference between a pair of orthogonally polarized incident waves. We believe that such a functional metalens has the potential to be used in systems such as optical instruments, drones, and mobile phone lenses in the future, greatly simplifying the equipment.

2. Unit Structure and Principle of the Bilayer Metalens

To implement a continuous varifocal metalens in the mid-infrared wave band, we designed a two-layer metasurface architecture as its meta-atom unit cell structure, as shown in Figure 1a. The meta unit structures of the top and bottom layers are composed of GSSe cylindrical nanopillars (Figure 1b) and Ge rectangular nanopillars (Figure 1c). Such a structure in Figure 1a may be fabricated as follows: First, a layer of Ge elements with a thickness of h_2 = 8 μm can be deposited on the MgF_2 substrate by thermal evaporation coating systems and magnetron sputtering machines. The Ge layer is then patterned using an electron beam exposure machine, followed by a high-density plasma etching process and enclosed in an h_3 = 9 μm-thick MgF_2 layer. Finally, a similar method can be used to fabricate the GSSe layer of thickness h_1 = 5.825 μm. The thickness of the substrate here is 4 μm. In particular, GSSe is a novel broadband transparent phase change material with a suitable refractive index contrast (Δn ≈ 0.32) and ultra-low extinction coefficient (k) in between the amorphous and crystalline states [46], providing a platform for designing a continuous varifocal lens. For the bottom layer material and substrate, Ge and MgF_2 were chosen with refractive indexes of about 4.004 and 1.18. From the focusing demonstration, we can see that the metalens focuses the x-polarized incident waves at F_{R1} and F_{L1} when GSSe is crystalline (Figure 1d). The focal length can be adjusted to F_{R2} and F_{L2} by changing GSSe from crystalline to amorphous (Figure 1e). Furthermore, we can also extend the phase change material (PCM) intermediate state to achieve a continuous varifocal metalens.

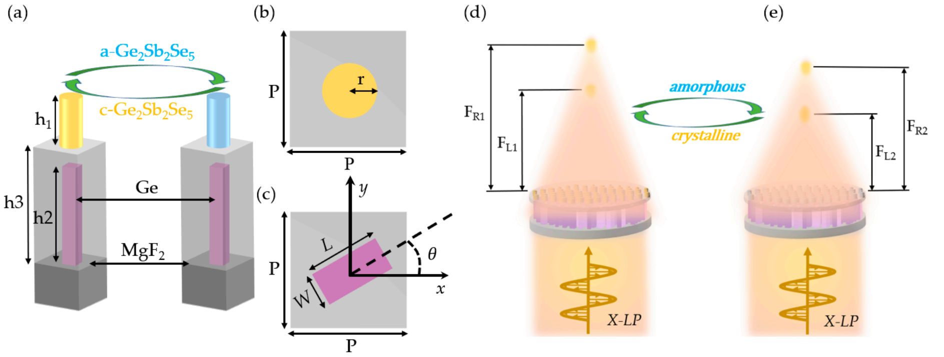

Figure 1. (**a**) The schematic diagram of the unit structure of the bilayer metalens. (**b**) Upper view of the GSSe unit nanopillar. (**c**) Upper view of the Ge rectangle unit nanopillar. The long and short axis of the Ge rectangle are *L* and *W*, and *θ* is the angle between the long axis and the horizontal direction. Artistic rendering of a bifocal varifocal metalens under *X-LP* wave excitations when GSSe is in the crystalline state (**d**) and the amorphous state (**e**).

To independently manipulate two orthogonal circular polarizations, the proposed metalens uses both geometric and propagation phases. The propagation phase is employed to impose a phase shift of $\beta = 2\pi nd/\lambda$ on the transmitted waves, where λ is the wavelength of the incident light, d is the distance of light wave propagation in the homogeneous medium, and n is the refractive index of the medium. Differently, the bottom layer of the device, composed of rectangular nanopillars with different L and W, imposes the phase shift combination of both the propagation and geometric phase on incident light. The geometric phase is expressed as $\Phi_{PB} = \pm 2\theta$, where θ is the angle of rotation of the nanofin with respect to the x-axis.

Theoretically, the following equation gives the necessary phase profile to concentrate an incident plane wave at a focal length:

$$P_i(x,y,F_i) = \frac{2\pi}{\lambda}\left(\sqrt{x^2+y^2+F_i{}^2}\right) - F_i \tag{1}$$

where F_i is the focal length and x and y represent the discretized spatial coordinates. The phase P_i might be the propagation phase, geometric phase, or a combination of both. In this work, for the unit structure Ge in which the optical axis forms an angle θ with the x-axis, $R(\theta)$ can be used to represent the rotation matrix of the rectangular coordinate system rotated counterclockwise by an angle θ [10]:

$$R(\theta) = \begin{pmatrix} \cos\theta & \sin\theta \\ -\sin\theta & \cos\theta \end{pmatrix} \tag{2}$$

Therefore, its transmission matrix in the rectangular coordinate system should be expressed as:

$$T_{LP} = R(\theta)\begin{pmatrix} t_{xx} & 0 \\ 0 & t_{yy} \end{pmatrix} R(-\theta) = \begin{pmatrix} t_{xx}\cos^2\theta + t_{yy}\sin^2\theta & (t_{yy}-t_{xx})\sin\theta\cos\theta \\ (t_{yy}-t_{xx})\sin\theta\cos\theta & t_{xx}\sin^2\theta + t_{yy}\cos^2\theta \end{pmatrix} \tag{3}$$

where t_{xx} denotes the polarization transmission coefficient in the x-direction when the direction of incidence of linearly polarized light is polarized along the x-axis, and the meaning of t_{yy} can be understood in the same way. By superimposing two circularly polarized lights with opposing helices, LP waves can be created. However, when the metalens is illuminated by a single circularly polarized wave, the transmission matrix can be obtained as follows:

$$T(\theta)_{cp} = \frac{1}{2}\begin{pmatrix} t_{LL} + t_{RR} & (t_{LL} - t_{RR})e^{i2\theta} \\ (t_{LL} - t_{RR})e^{-i2\theta} & t_{LL} + t_{RR} \end{pmatrix} \tag{4}$$

where t_{LL} and t_{RR} represent the complex transmission coefficients of the Ge nanopillars when the incident waves are LCP or RCP, respectively. Because we designed the Ge layer metasurface as a half-wave plate (HWP) such that $t_{LL} = -t_{RR}$, at this point, we can write $t_{LL} = A_{LL}e^{i\sigma LL}$, where σ_{LL} and A_{LL} represent the phase and amplitude, respectively. Therefore, Equation (4) can be expressed simply as [44]:

$$T(\theta)_{cp} = \begin{pmatrix} 0 & A_{LL}e^{i(\sigma_{LL}+2\theta)} \\ A_{LL}e^{i(\sigma_{LL}-2\theta)} & 0 \end{pmatrix} \tag{5}$$

For a light source that is circularly polarized, the Ge unit rotated by an angle θ can provide a phase distribution equal to $\sigma_{LL} \pm 2\theta$. Meanwhile, it is worth noting that the phase shift of the electromagnetic wave passing through the first layer metasurface is superimposed on the phase shift of the electromagnetic wave passing through the second layer metasurface to form the overall phase distribution of the metalens [44,51], which provides a method for improving the freedom of optical design. Based on the above analysis, the 3D finite-difference time domain (FDTD) method was used to simulate the transport properties of the Ge and GSSe unit structures. Figure 2a,b show the cross-polarized (T_{cross}) and co-polarized (T_{co}) transmittance as a function of the Ge unit structures L and W under RCP incidence. We would like the Ge nanostructures to function as an HWP, for example to convert RCP to LCP. Therefore, we define the polarization conversion rate as $PCR = T_{cross}/(T_{cross} + T_{co})$. From Figure 2, we can clearly see that the transmission amplitude of cross-polarization (yellow area in Figure 2a) is high, while the transmission amplitude of co-polarization (dark blue area in Figure 2b) is very low under RCP excitation. Here, we chose eight Ge unit nanopillars of different sizes to meet the maximum PCR as much as possible, and these eight units (the eight nanofins are marked by red circles) can also achieve a propagation phase coverage close to 2π under RCP excitation, as shown in (c) of Figure 2. The transmission and phase shift of cylindrical GSSe nanopillars can be seen in (d) of Figure 2. We placed the Ge unit on the square lattice with a lattice constant of 2.5 μm for a periodic arrangement. Compared with other micro-/nano-structures, the sub-wavelength grating structure provides more possibilities for efficient and highly integrated beam manipulation.

To engineer the metalens with two distinct foci, we designed the Ge layer metasurface to exhibit different focal lengths for incident light with opposite helicity. Then, according to Equation (1), we can know that, when RCP and LCP incident light irradiates the Ge layer metasurface, the focused phase profiles are $P_R\ (x, y, F_R)$ and $P_L\ (x, y, F_L)$, respectively. $\mathrm{F_R}$ and $\mathrm{F_L}$ are the corresponding focal lengths. More specifically, a Jones matrix J(x,y) that concurrently fulfills $J(x,y)\,|\,RCP\rangle = e^{iPR(x,y,F_R)}\,|\,LCP\rangle$ and $J(x,y)\,|\,LCP\rangle = e^{iPL(x,y,F_L)}\,|\,RCP\rangle$ can be used to represent the Ge layer metasurface. The required Jones matrix form can be written as [52]:

$$J(x,y) = \begin{pmatrix} \frac{e^{iP_L(x,y,F_L)}+e^{iP_R(x,y,F_R)}}{2} & \frac{ie^{iP_L(x,y,F_L)}-ie^{iP_R(x,y,F_R)}}{2} \\ \frac{ie^{iP_L(x,y,F_L)}-ie^{iP_R(x,y,F_R)}}{2} & \frac{-e^{iP_R(x,y,F_R)}-e^{iP_L(x,y,F_L)}}{2} \end{pmatrix} \tag{6}$$

Since the Ge unit structure rotated by an angle θ works as a half-wave plate, we can create a metasurface combining the propagation phase and geometric phase. Then, we define two Equations [10]:

$$P_R(x,y,F_R) = \sigma_{LL}(x,y) + 2\theta(x,y) \text{ and } \\ P_L(x,y,F_L) = \sigma_{LL}(x,y) - 2\theta(x,y) \tag{7}$$

Solving the two equations in Equation (7) leads to:

$$\sigma_{LL}(x,y) = \frac{P_R(x,y,F_R) + P_L(x,y,F_L)}{2} \tag{8}$$

$$2\theta(x,y) = \frac{P_R(x,y,F_R) - P_L(x,y,F_L)}{2} \tag{9}$$

2θ(*x*,*y*) and σ_{LL}(*x*,*y*) represent the PB phase and propagation phase provided by the rotated rectangular Ge meta-atoms, respectively. This enables any spatial point on the metalens to contribute to incident light modification. Furthermore, the GSSe layer metasurface is unaffected by incoming light polarization and provides a phase profile P_{GSSe}(*x*,*y*). Overall, it can be concluded that when the metalens is illuminated by RCP or LCP incident light, the final phase distribution has the following form [44]:

$$\begin{cases} P_{R(total)}(x,y) = \sigma_{LL}(x,y) + 2\theta(x,y) + P_{GSSe}(x,y) = P_R(x,y,F_R) + P_{GSSe}(x,y) \\ P_{L(total)}(x,y) = \sigma_{LL}(x,y) - 2\theta(x,y) + P_{GSSe}(x,y) = P_L(x,y,F_L) + P_{GSSe}(x,y) \end{cases} \tag{10}$$

$P_{R(total)}$(*x*,*y*) and $P_{L(total)}$(*x*,*y*) in Equation (10) can also meet the focusing Formula (1), and numerical calculations show that the bilayer metalens's focal length is nearly equal to the theoretical focal length (the focal length shifts less than 5%). Similar ultra-thin double-layer phase gradient metasurfaces can also pave the way for further research on high-performance achromatic metalenses [53].

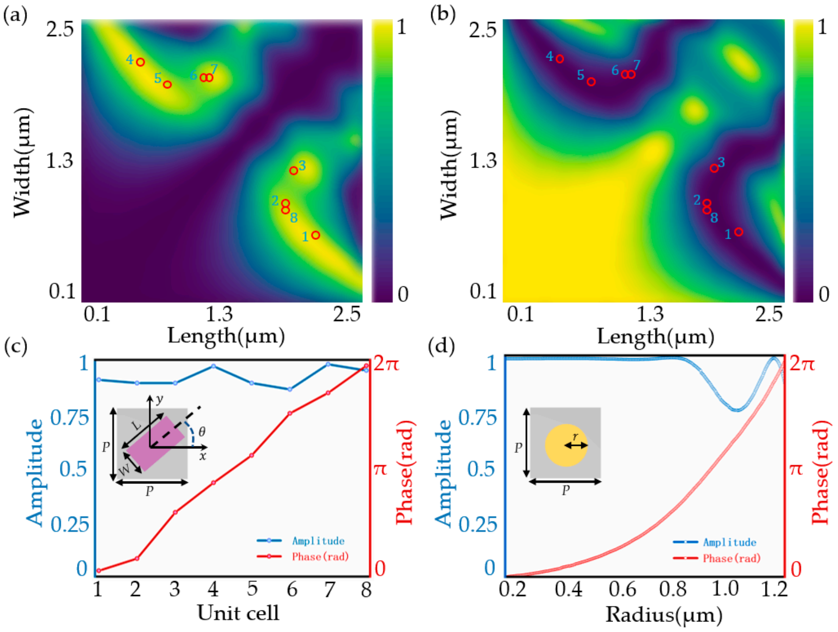

Figure 2. Transmission of cross-polarization (**a**) and co-polarization (**b**) was simulated under RCP incidence. The eight Ge nanofins marked by the red circles we selected are equivalent to the function of HWPs. (**c**) The phase change and specific transmission amplitude under RCP polarization incidence for the eight Ge cells selected (8 units in (**c**) correspond to the unit structure size marked with numbers 1-8 in (**a**)). (**d**) The phase and amplitude of GSSe cylindrical cells with different radii under the excitation of RCP polarization.

Besides, we can easily adjust the intensity ratio of the focus without redrawing the metalens when the metalens longitudinally focuses x-polarized incident light into two focal points. The proposed focal intensity controllability performance is verified by numerical simulations in the later discussion of the results.

3. Results and Discussion

3.1. Polarization-Dependent Varifocal Metalens

To intuitively exhibit the varifocal characteristics, a bilayer metalens was numerically investigated with x-polarized, RCP and LCP incident light, and the transmission properties of the metalens can be calculated with the three-dimensional FDTD method. The simulated focusing performance of the polarization-dependent metalens is illustrated in Figure 3. When the metalens is vertically illuminated by the x-LP wave, as shown in Figure 3a, two foci simultaneously appear on the z-axis. Meanwhile, LP waves can be split into two oppositely polarized circularly polarized waves [44]. Figure 3b,c show that the metalens will independently generate a single focal point if illuminated by RCP and LCP alone. From the simulation results, it can be concluded that the focal lengths are approximately 67.13 and 36.66 µm, and the corresponding numerical apertures (NAs) of the metalens are 0.51 and 0.74 according to the calculation of the numerical aperture $NA = sin[tan^{-1}(D/2F_i)]$.

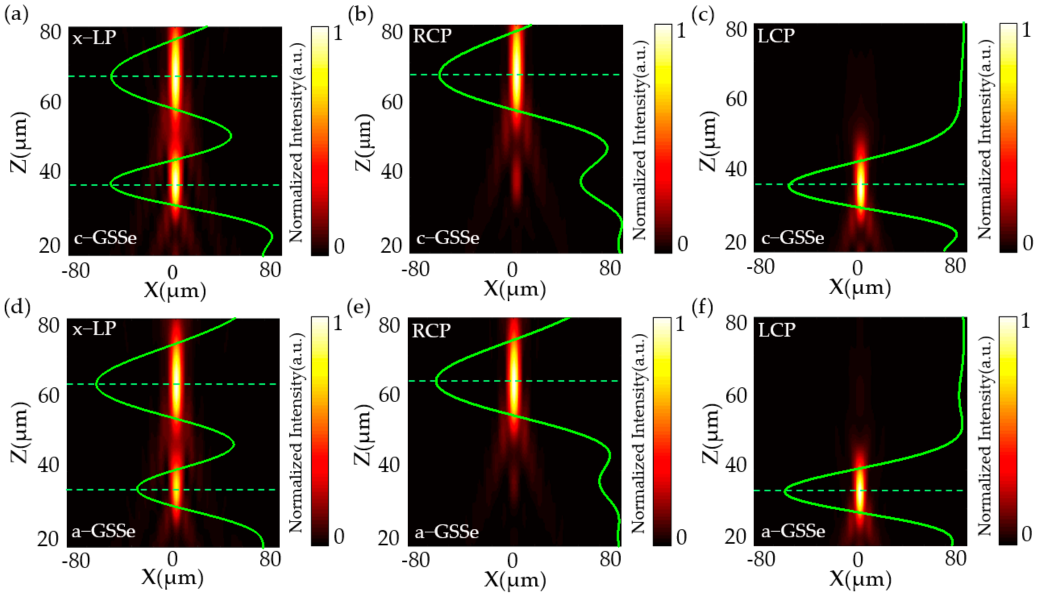

Figure 3. The intensity of the simulated electric field under three distinct polarization excitations When the GSSe phase change material is in the crystalline (x−LP (**a**), RCP (**b**), and LCP (**c**)) and amorphous (x−LP (**d**), RCP (**e**), and LCP (**f**)) states.

Similarly, when GSSe transitions from c-GSSe to a-GSSe, there are two new focal points generated under x-polarized light incidence, as shown in Figure 3d. Certainly, as can be seen from Figure 3e,f, the incident RCP or LCP light alone is also focused on new positions (62.91 µm and 33.84 µm), respectively, with the NAs of the metalens being 0.54 and 0.76. The green dashed and green solid curves represent the focused spot's central location and the cross-section's intensity distribution along the z-axis, respectively.

3.2. Polarization-Dependent Continuous Varifocal Metalens

Following the above analysis, we discuss only the crystalline and amorphous states of GSSe at specific wavelengths. Generally speaking, we can also consider the intermediate state of the phase change material GSSe, that is its partial crystalline state, so that a metalens with a continuously changing focal position can be achieved. The optical response of GSSe cylindrical nanopillars was simulated using the Lorentz–Lorenz relationship to characterize the dielectric constants of GSSe with various crystalline ratios:

$$\frac{\varepsilon_{eff}(\lambda)-1}{\varepsilon_{eff}(\lambda)+2}=m\times\frac{\varepsilon_{c-GSSe}(\lambda)-1}{\varepsilon_{c-GSSe}(\lambda)+2}+(1-m)\times\frac{\varepsilon_{a-GSSe}(\lambda)-1}{\varepsilon_{a-GSSe}(\lambda)+2} \tag{11}$$

The m in Equation (11) is the crystallization fraction of GSSe ranging from 1 to 0, and εc-GSSe(λ) and εa-GSSe(λ) approximate the dielectric constants of crystalline and amorphous GSSe scatterers, respectively. Then, we alter the crystalline fraction m of GSSe in the metalens, as indicated by the callout in Figure 4, m = 1(c-GSSe), m = 0.75, m = 0.5, m = 0.25, m = 0(a-GSSe). From Figure 4a,b, the phase shifts and transmission amplitudes with different crystalline fractions m as a function of the nanopillars' radius can be seen. When we decrease the crystalline fraction m of GSSe; the phase shift also becomes smaller, but still maintains a high transmission amplitude to achieve a better focusing effect.

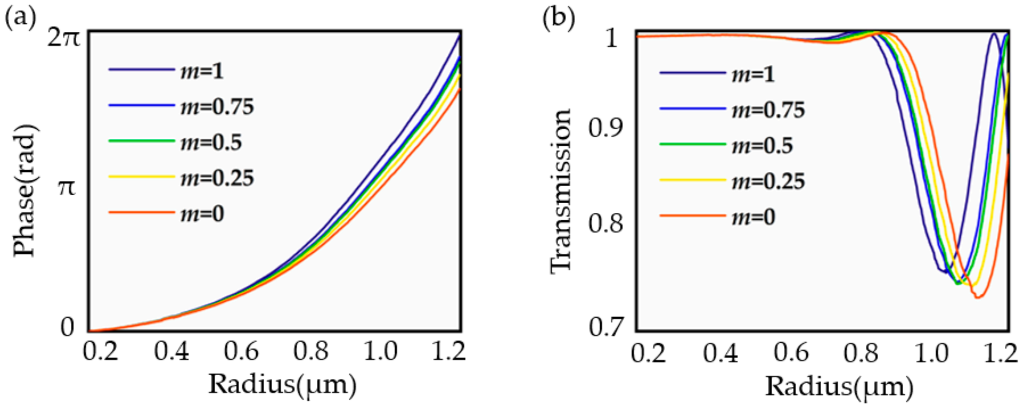

Figure 4. The optical response of the GSSe cylindrical nanopillars with different crystallization fractions m. The phase shifts (**a**) and transmission amplitudes (**b**) of the GSSe nanopillars with crystalline fraction m from 1 to 0 as a function of the nanopillars' radius.

Next, from Figure 5a,b, we can see that both bifocals and monofocals can be well-focused on the x-z plane. The intensity distribution results of the bifocals are shown in Figure 5a under the excitation of x-LP. The appearance of these two focal points comes partly from the focusing of the RCP waves, and the rest comes from the focusing of the LCP waves. From the focus demonstration of the output electric field, it can be seen that the two foci move farther as the crystallization fraction m increases gradually. Figure 5b plots the intensity profiles of a single focus corresponding to the incidence of RCP and LCP waves. Certainly, the changing behavior of the focal length of the monofocal is consistent with the bifocal. The focal length increases with increasing crystallization fraction m, while NA decreases. The zoom range of the focal point under RCP and LCP light illumination is about 4.22 μm and 2.81 μm. We can also see from Figure 5c that the specific position changes of Focus 1 (RCP) and Focus 2 (LCP) and the full-width at half-maximum (FWHM) correspond to the focus. The focal lengths of both foci increase linearly with m. Figure 5d reveals the focusing efficiency corresponding to the focus of the continuous zoom metalens in Figure 5c. We define the focusing efficiency as the ratio of the sum of the light field intensity on the focal plane to the sum of the light field intensity of the transmitted beam on the metalens surface. Because the phase change material GSSe has low loss, the focusing efficiency is about 59% and 48% under the excitation of the RCP wave and LCP wave. Such a double-layer structure may also add more metasurface layers or change the dielectric thickness to achieve higher NA and larger focusing efficiency [54]. This enables the idea of the continuous zoom metalens to be validated in the mid-infrared, while the proposed polarization-dependent continuous varifocal metalens also has potential applications in biological and medical instruments, optical imaging systems, and compact optical devices.

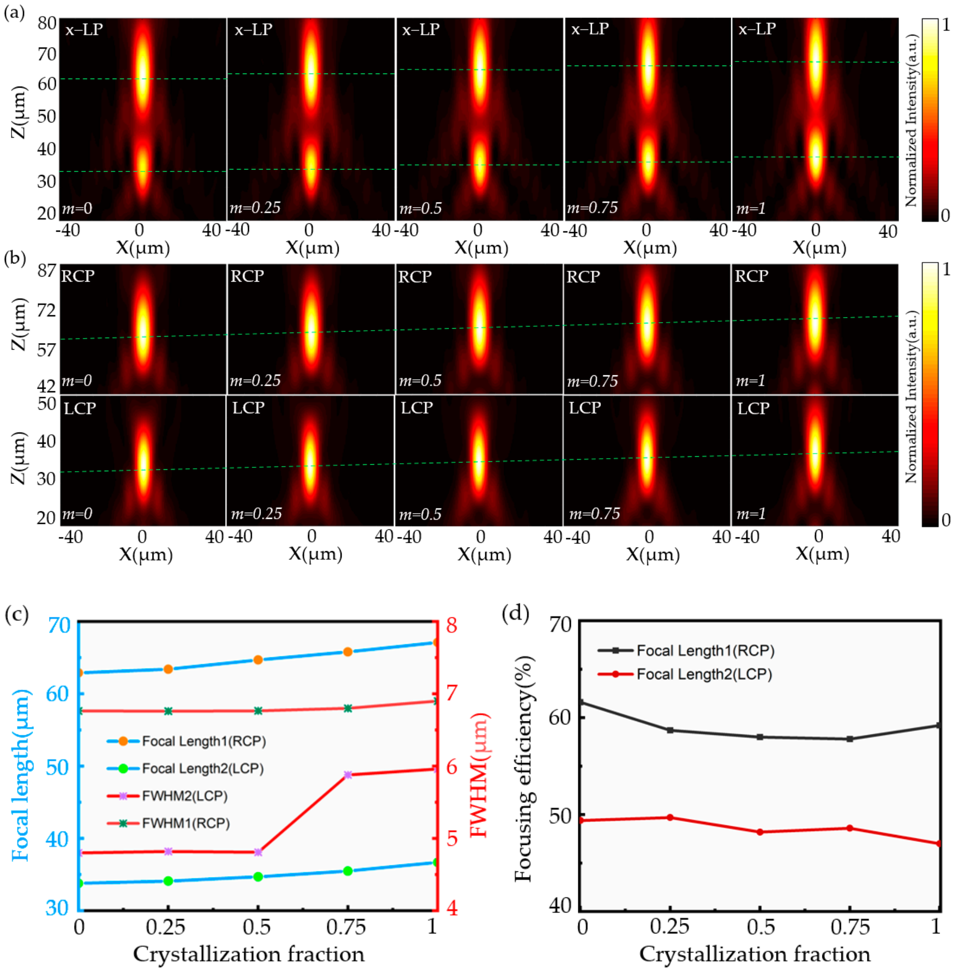

Figure 5. Demonstration of electric field strength in the x−z plane under x-polarized light (**a**), right−handed circular and left−handed circular light incident (**b**) when the crystalline fraction m of GSSe varies from 0 to 1. (**c**) The focal length and FWHM of the metalens correspond to different m under the excitation of RCP and LCP. (**d**) The corresponding focusing efficiencies of the foci in (**c**).

3.3. Bifocal Metalens with Adjustable Intensity Ratios

For the design of the bifocal metalens, an important factor we need to consider is the intensity ratio at the focal points. We know that two orthogonally polarized beams can be superimposed into an elliptically polarized beam, and we can also decompose the LP waves into two oppositely directed RCP and LCP waves. More specifically, our designed metalens can well focus the RCP and LCP waves at FR1 and FL1 independently, and the intensity distribution of the focus on the x-z plane is shown in Figure 6a,b. The intensity profiles of the two foci in the x-y plane are shown in Figure 6c,d, corresponding to the FWHM in Figure 6e,f, where the value of FWHM reflects the size of the focal spot.

To demonstrate that the intensity ratio between the above two focal points can be modulated, we simulated the intensity contrast map of the two focal points in the far-field domain with FDTD software, as shown in Figure 7a. Here, we used Ex and Ey beams with equal amplitude; the directions of vibration are perpendicular to each other and a phase difference of δ as the total incident beam. Ex and Ey represent the components of the electromagnetic waves on the x- and y-axis, and $\delta = \varphi x - \varphi y$ represents the phase difference between the phase on the y-component and the phase on the x-component. When $\delta > 0$, it is defined as right-handed elliptically polarized light; otherwise, $\delta < 0$ means left-handed elliptically polarized light. The deeper meaning of judging the rotation of the incident beam is as follows: it is right-handed elliptically polarized light when the phase of the y-component is earlier than the x-phase component; when the y-component's phase lags behind the x-component's phase, we can think of it as left-handed elliptically polarized light. If δ = 0 corresponds to linearly polarized light, when $\delta = \pm\pi/2$, it corresponds to RCP and LCP light, and the light propagation direction is along the positive direction of the z-axis. Therefore, we flexibly adjust the ellipticity of the incident electromagnetic wave by changing the phase difference δ to achieve different focus intensity contrasts. Figure 7a shows the demonstration of the comparison of foci intensity at different phase differences δ, from which the intensity evolution of the two foci along the z-axis can be seen. From the simulation results, when δ gradually increases from −90° to 90° (the change interval is 30°, the electric field intensity distribution clearly shows that the intensity contrast of the two foci has changed. Then, from the intensity profile in Figure 7b, it is shown that the corresponding intensity contrasts at different δ are 0.03, 0.15, 0.45, 1.02,1.97,3.32, and 4.26.

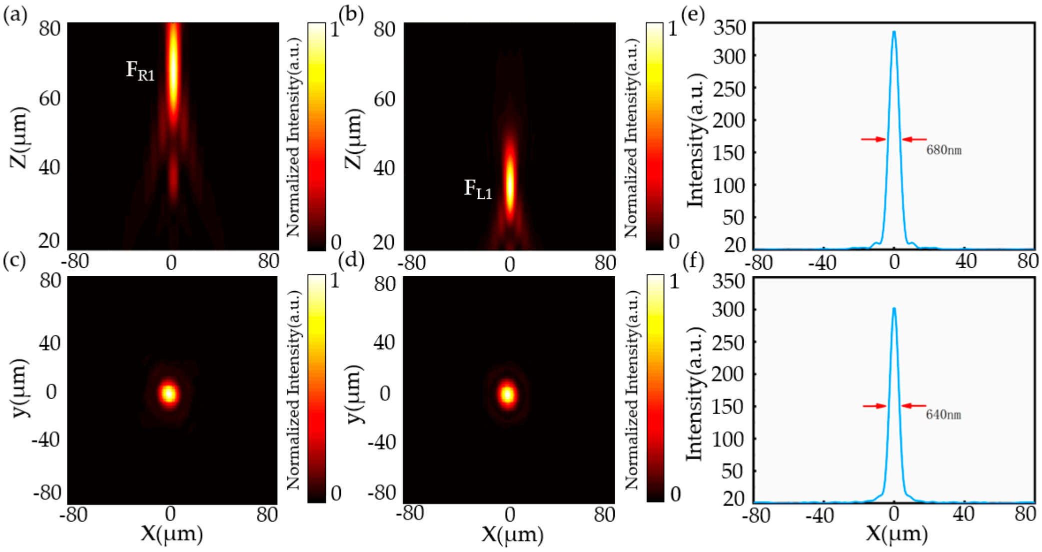

Figure 6. Demonstration of the intensity of the simulated metalens in the x−z and x−y planes under RCP (**a**,**c**) and LCP (**b**,**d**) incident light, when the GSSe phase change material is crystalline. (**e**,**f**) The FWHM values corresponding to the focal spot in (**c**) and (**d**) are 680 nm and 640 nm.

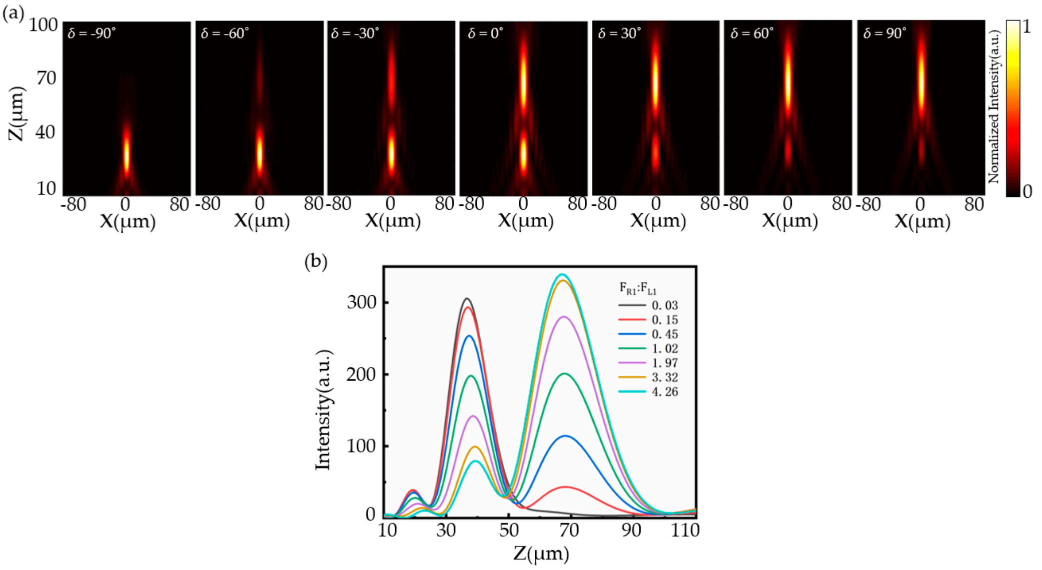

Figure 7. (**a**) The relative electric field intensity profiles of two focal points in the x−z plane for the different phase difference δ. (**b**) Demonstration of intensity distribution at the longitudinal focal length.

4. Conclusions

In conclusion, we designed a phase-change-material (GSSe)-enabled mid-infrared reconfigurable bilayer metalens by simultaneously harnessing the propagation and geometric phase. Our numerical simulation results show that the proposed metalens could not only achieve continuous zooming, but also control the intensity ratio of the focus. The moving range of the focal length under the irradiation of RCP and LCP incident light is about 4.22 µm and 2.81 µm, and the intensity ratios of bifocals vary from about 0.03 to 4.26. The focusing efficiency can reach about 59% and 48% under RCP and LCP wave excitation. The design methodology employed in the double-layer structure may also be extended to multiple layers to achieve complex functions with more degrees of freedom with phase control, and the proposed bilayer metalens has great potential in imaging platforms, biomedical, optical tomography, and other fields.

Author Contributions: Conceptualization and model, L.S.; numerical simulation, L.S. and K.Z.; writing—original draft preparation, L.S. and F.Z.; investigation and formal analysis F.Z.; writing—review and editing, L.S., Y.G. and B.W.; project administration and resources, X.S. All authors have read and agreed to the published version of the manuscript.

Funding: This work was supported by National Natural Science Foundation of China (Grant No. U21A2056).

Institutional Review Board Statement: Not applicable.

Informed Consent Statement: Not applicable.

Data Availability Statement: The data supporting the findings of this study are available within the article.

Conflicts of Interest: The authors declare no conflict of interest.

References

1. Yu, N.; Genevet, P.; Kats, M.A.; Aieta, F.; Tetienne, J.P.; Capasso, F.; Gaburro, Z. Light Propagation with Phase Discontinuities: Generalized Laws of Reflection and Refraction. *Science* **2011**, *334*, 333–337. [CrossRef] [PubMed]
2. Decker, M.; Staude, I.; Falkner, M.; Dominguez, J.; Neshev, D.N.; Brener, I.; Pertsch, T.; Kivshar, Y.S. High-Efficiency Dielectric Huygens' Surfaces. *Adv. Opt. Mater.* **2015**, *3*, 813–820. [CrossRef]
3. Ou, K.; Yu, F.; Li, G.; Wang, W.; Miroshnichenko, A.E.; Huang, L.J.; Wang, P.; Li, T.; Li, Z.; Chen, X.S.; et al. Mid-infrared polarization-controlled broadband achromatic metadevice. *Sci. Adv.* **2020**, *6*, eabc0711. [CrossRef] [PubMed]
4. Devlin, R.C.; Ambrosio, A.; Rubin, N.A.; Mueller, J.P.B.; Capasso, F. Arbitrary spin-to–orbital angular momentum conversion of light. *Science* **2017**, *358*, 896–901. [CrossRef] [PubMed]
5. Arbabi, E.; Arbabi, A.; Kamali, S.M.; Horie, Y.; Faraon, A. Multiwavelength polarization-insensitive lenses based on dielectric metasurfaces with meta-molecules. *Optica* **2016**, *3*, 628–633. [CrossRef]
6. Wang, S.; Wu, P.C.; Su, V.C.; Lai, Y.C.; Chen, M.K.; Kuo, H.Y.; Chen, B.H.; Chen, Y.H.; Huang, T.T.; Wang, J.H.; et al. A broadband achromatic metalens in the visible. *Nat. Nanotechnol.* **2018**, *13*, 227–232. [CrossRef]
7. Zhou, K.S.; Wang, B.X.; Tang, S.W.; Gao, Y.X.; Liu, S.; Sheng, Y.; Chen, J.J.; Dai, S.X.; Shen, X. Mid-infrared biomimetic moth-eye-shaped polarization-maintaining and angle-insensitive metalens. *Opt. Express* **2022**, *30*, 12048–12060. [CrossRef]
8. Wang, Y.L.; Fan, Q.B.; Xu, T. Design of high efficiency achromatic metalens with large operation bandwidth using bilayer architecture. *Opto-Electron. Adv.* **2021**, *4*, 200008. [CrossRef]
9. Zuo, H.J.; Choi, D.Y.; Gai, X.; Ma, P.; Xu, L.; Neshev, D.N.; Zhang, B.; Luther-Davies, B. High-Efficiency All-Dielectric Metalenses for Mid-Infrared Imaging. *Adv. Opt. Mater.* **2017**, *5*, 1700585. [CrossRef]
10. Badloe, T.; Kim, I.; Kim, Y.; Kim, J.; Rho, J. Electrically Tunable Bifocal Metalens with Diffraction-Limited Focusing and Imaging at Visible Wavelengths. *Adv. Sci.* **2021**, *8*, 2102646. [CrossRef]
11. Shan, D.; Xu, N.X.; Gao, J.S.; Song, N.T.; Liu, H.; Tang, Y.; Feng, X.G.; Wang, Y.S.; Zhao, Y.; Chen, X.; et al. Design of the all-silicon long-wavelength infrared achromatic metalens based on deep silicon etching. *Opt. Express* **2022**, *30*, 13616–13629. [CrossRef]
12. Ding, F.; Chang, B.D.; Wei, Q.S.; Huang, L.L.; Guan, X.W.; Bozhevolnyi, S.I. Versatile Polarization Generation and Manipulation Using Dielectric Metasurfaces. *Laser Photonics Rev.* **2020**, *14*, 2000116. [CrossRef]
13. Ren, H.; Fang, X.Y.; Jang, J.; Burger, J.; Rho, J.; Maier, S.A. Complex-amplitude metasurface-based orbital angular momentum holography in momentum space. *Nat. Nanotechnol.* **2020**, *15*, 948–955. [CrossRef]
14. Xu, J.; Li, R.Q.; Wang, S.Y.; Han, T.C. Ultra-broadband linear polarization converter based on anisotropic metasurface. *Opt. Express* **2018**, *26*, 26235–26241. [CrossRef]

15. Yu, N.F.; Aieta, F.; Genevet, P.; Kats, M.A.; Gaburro, Z.; Capasso, F. A broadband, background-free quarter-wave plate based on plasmonic metasurfaces. *Nano Lett.* **2012**, *12*, 6328–6333. [CrossRef]
16. Teng, S.; Zhang, Q.; Wang, H.; Liu, L.X.; Lv, H. Conversion between polarization states based on a metasurface. *Photonics Res.* **2019**, *7*, 246. [CrossRef]
17. Genevet, P.; Yu, N.; Aieta, F.; Lin, J.; Kats, M.A.; Blanchard, R.; Scully, M.O.; Gaburro, Z.; Capasso, F. Ultra-thin plasmonic optical vortex plate based on phase discontinuities. *Appl. Phys. Lett.* **2012**, *100*, 013101. [CrossRef]
18. Ou, K.; Li, G.H.; Li, T.X.; Yang, H.; Yu, F.L.; Chen, J.; Zhao, Z.Y.; Cao, G.G.; Chen, X.S.; Lu, W. High efficiency focusing vortex generation and detection with polarization-insensitive dielectric metasurfaces. *Nanoscale* **2018**, *10*, 19154–19161. [CrossRef]
19. Wang, W.; Li, Y.; Guo, Z.Y.; Li, R.Z.; Zhang, J.R.; Zhang, A.J.; Qu, S.L. Ultra-thin optical vortex phase plate based on the metasurface and the angular momentum transformation. *J. Opt.* **2015**, *17*, 045102. [CrossRef]
20. Ding, F.; Chen, Y.T.; Bozhevolnyi, S.I. Focused vortex-beam generation using gap-surface plasmon metasurfaces. *Nanophotonics* **2020**, *9*, 371–378. [CrossRef]
21. He, J.W.; Ye, J.S.; Wang, X.K.; Kan, Q.; Zhang, Y. A broadband terahertz ultrathin multi-focus lens. *Sci. Rep.* **2016**, *6*, 28800. [CrossRef] [PubMed]
22. Chen, X.Z.; Chen, M.; Mehmood, M.Q.; Wen, D.; Yue, F.; Qiu, C.W.; Zhang, S. Longitudinal Multifoci Metalens for Circularly Polarized Light. *Adv. Opt. Mater.* **2015**, *3*, 1201–1206. [CrossRef]
23. Wang, Q.; Zhang, X.Q.; Plum, E.; Xu, Q.; Wei, M.G.; Xu, Y.H.; Zhang, H.F.; Liao, Y.; Gu, J.Q.; Han, J.G.; et al. Polarization and Frequency Multiplexed Terahertz Meta-Holography. *Adv. Opt. Mater.* **2017**, *5*, 1700277. [CrossRef]
24. Ji, R.; Chen, K.J.; Ni, Y.J.; Hua, Y.N.; Long, K.; Zhuang, S.L. Dual-Focuses Metalens for Copolarized and Cross-Polarized Transmission Waves. *Adv. Cond. Matter Phys.* **2018**, *2018*, 2312694. [CrossRef]
25. Ee, H.S.; Agarwal, R. Tunable Metasurface and Flat Optical Zoom Lens on a Stretchable Substrate. *Nano Lett.* **2016**, *16*, 2818–2823. [CrossRef] [PubMed]
26. Kamali, S.M.; Arbabi, E.; Arbabi, A.; Horie, Y.; Faraon, A. Highly tunable elastic dielectric metasurface lenses. *Laser Photonics Rev.* **2016**, *10*, 1002–1008. [CrossRef]
27. Wei, S.B.; Cao, G.Y.; Lin, H.; Yuan, X.C.; Somekh, M.; Jia, B. A Varifocal Graphene Metalens for Broadband Zoom Imaging Covering the Entire Visible Region. *ACS Nano* **2021**, *15*, 4769–4776. [CrossRef]
28. Cui, Y.; Zheng, G.X.; Chen, M.; Zhang, Y.L.; Yang, Y.; Tao, J.; He, T.T.; Li, Z.L. Reconfigurable continuous-zoom metalens in visible band. *Chin. Opt. Lett.* **2019**, *17*, 111603. [CrossRef]
29. Iwami, K.; Ogawa, C.; Nagase, T.; Ikezawa, S. Demonstration of focal length tuning by rotational varifocal moire metalens in an ir-A wavelength. *Opt. Express* **2020**, *28*, 35602–35614. [CrossRef]
30. Wang, C.; Sun, Y.; Zhang, Q.B.; Yu, Z.Q.; Tao, C.N.; Zhang, J.L.; Wu, F.; Wu, R.; Zheng, Z. Continuous-zoom bifocal metalens by mutual motion of cascaded bilayer metasurfaces in the visible. *Opt. Express* **2021**, *29*, 26569–26585. [CrossRef]
31. Colburn, S.; Zhan, A.; Majumdar, A. Varifocal zoom imaging with large area focal length adjustable metalenses. *Optica* **2018**, *5*, 825. [CrossRef]
32. Arbabi, E.; Arbabi, A.; Kamali, S.M.; Horie, Y.; Faraji-Dana, M.S.; Faraon, A. MEMS-tunable dielectric metasurface lens. *Nat. Commun.* **2018**, *9*, 812. [CrossRef]
33. Han, Z.Y.; Colburn, S.; Majumdar, A.; Bohringer, K.F. MEMS-actuated metasurface Alvarez lens. *Microsyst. Nanoeng.* **2020**, *6*, 79. [CrossRef]
34. Meng, C.; Thrane, P.C.V.; Ding, F.; Gjessing, J.; Thomaschewski, M.; Wu, C.; Dirdal, C.; Bozhevolnyi, S.I. Dynamic piezoelectric MEMS-based optical metasurfaces. *Sci. Adv.* **2021**, *7*, 5639. [CrossRef]
35. Zhou, S.H.; Shen, Z.X.; Li, X.N.; Ge, S.J.; Lu, Y.Q.; Hu, W. Liquid crystal integrated metalens with dynamic focusing property. *Opt. Lett.* **2020**, *45*, 4324–4327. [CrossRef]
36. Bosch, M.; Shcherbakov, M.R.; Won, K.; Lee, H.S.; Kim, Y.; Shvets, G. Electrically Actuated Varifocal Lens Based on Liquid-Crystal-Embedded Dielectric Metasurfaces. *Nano Lett.* **2021**, *21*, 3849–3856. [CrossRef]
37. Shen, Z.X.; Zhou, S.H.; Li, X.N.; Ge, S.J.; Chen, P.; Hu, W.; Lu, Y.Q. Liquid crystal integrated metalens with tunable chromatic aberration. *Adv. Photonics* **2020**, *2*, 036002. [CrossRef]
38. Ding, P.; Li, Y.; Shao, L.; Tian, X.M.; Wang, J.Q.; Fan, C.Z. Graphene aperture-based metalens for dynamic focusing of terahertz waves. *Opt. Express* **2018**, *26*, 28038–28050. [CrossRef]
39. He, J.J.; Chen, R.K.; Li, Y.F.; Chen, S.P.; Liu, Z.M.; Zhang, Q.M. Graphene metalens with dynamic focusing and plane focusing in the terahertz range. *Appl. Opt.* **2021**, *60*, 5752–5758. [CrossRef]
40. Zhang, Z.K.; Qi, X.Q.; Zhang, J.F.; Guo, C.C.; Zhu, Z.H. Graphene-enabled electrically tunability of metalens in the terahertz range. *Opt. Express* **2020**, *28*, 28101–28112. [CrossRef]
41. Li, S.Y.; Zhou, C.B.; Ban, G.X.; Wang, H.; Lu, H.; Wang, Y. Active all-dielectric bifocal metalens assisted by germanium antimony telluride. *J. Phys. D* **2019**, *52*, 095106. [CrossRef]
42. Qin, S.; Xu, N.; Huang, H.; Jie, K.Q.; Liu, H.Z.; Guo, J.P.; Meng, H.Y.; Wang, F.Q.; Yang, X.B.; Wei, Z.C. Near-infrared thermally modulated varifocal metalens based on the phase change material Sb2S3. *Opt. Express* **2021**, *29*, 7925–7934. [CrossRef] [PubMed]
43. Shalaginov, M.Y.; An, S.; Zhang, Y.F.; Yang, F.; Su, P.; Liberman, V.; Chou, J.B.; Roberts, C.M.; Kang, M.; Rios, C.; et al. Reconfigurable all-dielectric metalens with diffraction-limited performance. *Nat. Commun.* **2021**, *12*, 1225. [CrossRef] [PubMed]

44. Wang, Y.Q.; Chen, L.; Tang, S.W.; Xu, P.P.; Ding, F.; Fang, Z.R.; Majumdar, A. Helicity-dependent continuous varifocal metalens based on bilayer dielectric metasurfaces. *Opt. Express* **2021**, *29*, 39461–39472. [CrossRef] [PubMed]
45. Yin, X.H.; Steinle, T.; Huang, L.L.; Taubner, T.; Wuttig, M.; Zentgraf, T.; Giessen, H. Beam switching and bifocal zoom lensing using active plasmonic metasurfaces. *Light Sci. Appl.* **2017**, *6*, 17016. [CrossRef]
46. Zhang, Y.F.; Chou, J.B.; Li, J.Y.; Li, H.S.; Du, Q.Y.; Yadav, A.; Zhou, S.; Shalaginov, M.Y.; Fang, Z.R.; Zhong, H.K.; et al. Broadband transparent optical phase change materials for high-performance nonvolatile photonics. *Nat. Commun.* **2019**, *10*, 4279.
47. Zhang, Y.F.; Li, J.Y.; Chou, J.B.; Fang, Z.R.; Yadav, A.; Lin, H.; Du, Q.; Michon, J.; Han, Z.H.; Huang, Y.Z.; et al. *Broadband Transparent Optical Phase Change Materials*; Optica Publishing Group: San Jose, CA, USA, 2017; p. JTh5C-4.
48. Lin, R.G.; Li, X.H. Multifocal metalens based on multilayer Pancharatnam–Berry phase elements architecture. *Opt. Lett.* **2019**, *44*, 2819–2822.
49. Chen, L.; Hao, Y.; Zhao, L.; Wu, R.; Liu, Y.; Wei, Z.C.; Xu, N.; Li, Z.T.; Liu, H.Z. Multifunctional metalens generation using bilayer all-dielectric metasurfaces. *Opt. Express* **2021**, *29*, 9332–9345. [CrossRef]
50. Tian, S.N.; Guo, H.M.; Hu, J.B.; Zhuang, S.L. Dielectric longitudinal bifocal metalens with adjustable intensity and high focusing efficiency. *Opt. Express* **2019**, *27*, 680–688. [CrossRef]
51. Zhou, Y.; Kravchenko, I.I.; Wang, H.; Nolen, J.R.; Gu, G.; Valentine, J. Multilayer Noninteracting Dielectric Metasurfaces for Multiwavelength Metaoptics. *Nano Lett.* **2018**, *18*, 7529–7537.
52. Liu, M.Z.; Huo, P.C.; Zhu, W.Q.; Zhang, C.; Zhang, S.; Song, M.W.; Zhang, S.; Zhou, Q.W.; Chen, L.; Lezec, H.J.; et al. Broadband generation of perfect Poincare beams via dielectric spin-multiplexed metasurface. *Nat. Commun.* **2021**, *12*, 2230. [CrossRef]
53. Liu, Y.Q.; Ren, Z.R.; Shu, Y.C.; Wu, L.J.; Sun, J.H.; Cai, H.; Zhang, X.T.; Lu, L.; Qi, K.N.; Li, L.S.; et al. Broadband, large-numerical-aperture and high-efficiency microwave metalens by using a double-layer transmissive metasurface. *Appl. Phys. Express* **2022**, *15*, 014003. [CrossRef]
54. Liu, Y.Q.; Sun, J.H.; Shu, Y.C.; Wu, L.J.; Lu, L.; Qi, K.N.; Che, Y.X.; Li, L.S.; Yin, H.C. High numerical aperture and large focusing efficiency metalens based on multilayer transmitarray elements. *Opt. Lasers Eng.* **2021**, *147*, 106734. [CrossRef]